

Stress Distribution and Relaxation in Cellulose Nanocrystal-Enhanced GFRP Composites Under Sustained Loading

Ehsan Ataei^a, Younes Mohammadi^{a,*}, Ali Akbar Pasha Zanoosi^a

^a Department of Mechanical Engineering, Faculty of Industrial & Mechanical Engineering, Islamic Azad University, Qazvin Branch, Qazvin, Iran Received 10 October 2024, Accepted 05 December 2024

Abstract

The viscoelastic nature of the polymer matrix in Glass Fiber Reinforced Polymer (GFRP) composites results in complex time-dependent stress redistribution under sustained loads, a critical factor for maintaining long-term structural integrity. This study presents a comprehensive experimental and numerical investigation into the creep behavior and stress relaxation mechanisms of GFRP composites, with a specific focus on the enhancement effects of cellulose nanocrystals (CNCs). The Norton-Bailey creep model was rigorously calibrated for a DGEBA epoxy matrix, demonstrating exceptional predictive accuracy ($R^2 > 0.95$) with a creep exponent of $n \approx 1.082$. The Burgers model was employed to capture the time-dependent behavior of the fiber-matrix system. Micromechanical analysis via Finite Element Analysis (FEA) of high-fidelity Representative Volume Elements (RVEs) subjected to a sustained equivalent stress of 100 MPa for 7200 seconds revealed profound, orientation-dependent stress evolution. In 0° laminates, fiber stress decreased by 17% while matrix stress increased by 340%, signifying dramatic load transfer. Incorporation of 1.0 wt% CNCs was identified as optimal, reducing stress concentration factors by 17–36% and enhancing stress field homogeneity across all fiber orientations (0° , 45° , 90°) by improving interfacial bonding and matrix stiffness. This validated multi-scale framework provides critical insights and a reliable predictive tool for designing durable, high-performance composite structures in aerospace, automotive, and civil infrastructure applications.

Keywords: GFRP Composites; Cellulose Nanocrystals (CNCs); Creep; Stress Relaxation; Finite Element Analysis (FEA); Representative Volume Element (RVE); Norton-Bailey Model; Burgers Model; Micromechanics

1. Introduction

The excellent specific strength and corrosion resistance of Glass Fiber Reinforced Polymer (GFRP) composites have led to their proliferation in long-term, load-bearing applications across aerospace, wind energy, and civil infrastructure [1, 2]. A paramount design consideration for such applications is the time-dependent mechanical response, or creep, of the composite. This behavior originates from the inherent viscoelasticity of the thermosetting polymer matrix, which, under sustained load, undergoes gradual deformation, leading to a dynamic redistribution of stress between the stiff, elastic fibers and the compliant, viscoelastic matrix [3, 4]. This stress relaxation can precipitate premature matrix cracking, interfacial debonding, and ultimately, a reduction in the service life of the structure.

Accurately predicting this phenomenon requires a multiscale approach: a validated constitutive model for the matrix and a micromechanical understanding of stress evolution at the fiber-matrix level. The Norton-Bailey power-law model is frequently employed to characterize the steady-state creep of metallic and polymeric materials [5, 6], but its parameters must be precisely determined for the specific composite system. Furthermore, while the macroscopic creep of composites is well-documented, the intricate, time-dependent load transfer mechanisms at the micro-scale are less understood. Recent multi-scale modeling efforts have begun to bridge this gap, yet many rely on simplified linear viscoelasticity or lack direct experimental validation for the matrix behavior [13]. Recent advancements have explored nanoscale reinforcements to mitigate these detrimental time-

reinforcements to mitigate these detrimental timedependent effects. Cellulose Nanocrystals (CNCs), derived from renewable resources, offer exceptional stiffness, high aspect ratio, and a reactive surface, making them ideal candidates for enhancing polymer matrices [7, 8]. By improving matrix stiffness and fiber-matrix adhesion, CNCs have the potential to restrain viscoelastic flow and homogenize stress distributions, thereby performance. long-term improving Contemporary research has expanded into hybrid nanomaterial systems, combining CNCs with other nano-reinforcements like graphene oxide for synergistic effects, though the fundamental mechanisms in single-reinforcement systems require further elucidation at the micro-mechanical level [14].

This work presents a holistic investigation that bridges this gap. The primary objectives are twofold: (1) to experimentally characterize and validate the Norton-Bailey creep model for a neat epoxy matrix and its CNCenhanced nanocomposites, and (2) to employ advanced numerical simulations using Representative Volume Elements (RVEs) to elucidate the dynamic stress distribution and relaxation phenomena across critical fiber orientations (0°, 45°, and 90°). The insights gleaned provide a robust scientific basis for the design of next-generation, durable GFRP composites.

2. Materials And Experimental Methods

2.1. Materials

- 2.1.1 Polymer Matrix: A diglycidyl ether of bisphenol-A (DGEBA) epoxy resin (KER 828) was used as the matrix material. The curing agent was triethylenetetramine (TETA), mixed at a stoichiometric ratio of 100:15 (resin: hardener by weight).
- 2.1.2 Reinforcement: Unidirectional E-glass fibers (Corning Owens) with a filament diameter of 16 μ m, an areal weight of 200 g/m², and a tensile strength of 3400 MPa were used as the primary reinforcement.
- 2.1.3 Nanomaterial: Cellulose nanocrystals (CNCs) were produced from raw cotton linters via chemical processing (acid hydrolysis). Characterization confirmed average dimensions of 150 \pm 20 nm in length and 15 \pm 3 nm in diameter.

2.2. Nanocomposite and GFRP Laminate Fabrication

CNCs were incorporated into the epoxy resin at concentrations of 0, 0.5, 1.0, and 1.5 wt% using a hybrid dispersion protocol. This involved initial high-speed mechanical mixing (2500 rpm, 5 min) followed by ultrasonic treatment (20 min, 60% amplitude) with the temperature maintained below 40°C using an ice bath to prevent thermal degradation. After dispersion, the TETA hardener was added and mixed thoroughly.

Composite laminates with a fiber volume fraction of 60% were fabricated using Vacuum-Assisted Resin Transfer Molding (VARTM). The CNC-epoxy mixture was infused into the unidirectional glass fiber preform under a vacuum of 0.85 bar. The laminates were cured at ambient conditions (26 \pm 1°C) for 48 hours. Specimens for mechanical testing were laser-cut into dumbbell shapes (ASTM D638 Type IV).

2.3. Mechanical and Creep Testing

All mechanical tests were conducted on a Zwick Z010 universal testing machine. Quasi-static tensile tests were performed at a crosshead speed of 5 mm/min to determine the Young's modulus and ultimate tensile strength. Young's modulus was calculated from the slope of the linear elastic portion of the stress-strain curve within the small strain range (0.04%–0.05%). Environmental conditions were maintained at 26°C \pm 1°C and 50% \pm 5% relative humidity.

Uniaxial creep tests were performed on both neat epoxy and CNC/epoxy nanocomposite specimens according to ASTM D2990. The applied load in the creep tests for each specimen was determined as 20–30% of the ultimate static load to study creep behavior without causing damage. Tests were conducted at multiple stress levels (2.5, 5, 10, and 20 MPa) for a duration of 7200 seconds (2 hours).

Strain was continuously monitored using high-precision extensometers to accurately capture primary and secondary creep regimes.



Fig .1. Unidirectional GFRP sheets in 3 different angles: (a) 45, (b) 90, and (c) 0

3. Constitutive Modeling And Numerical Framework

3.1. Constitutive Models and Parameter Determination

3.1.1. Epoxy Matrix:

Norton-Bailey Creep Model

The time-dependent deformation of the epoxy matrix was modeled using the Norton-Bailey power-law creep equation

$$\dot{\varepsilon_c} = A\sigma^n t^m \tag{1}$$

where $\dot{\varepsilon}_c$ is the creep strain rate, σ is the applied stress, t is time, and A, n, and m are material-specific constants. Parameter Determination:

The Norton-Bailey parameters (A, m, n) were extracted by fitting the experimental creep curves at different stress levels (2.5-20 MPa) using nonlinear optimization algorithms in MATLAB. The effect of various CNC concentrations (0.5, 1.0, and 1.5 wt%) on the Norton-Bailey parameters was analyzed by fitting the creep curves of neat and CNC-reinforced epoxy specimens to the experimental data. This analysis enabled quantitative comparison of the effect of CNC addition on the matrix's viscoelastic properties.

Model Justification: The Norton-Bailey model was selected because, under constant temperature conditions, it can accurately describe time-dependent creep deformation in the steady-state phase of polymeric materials.

Supply some 5–6 keywords, separated with semicolons.

Table 1 Norton-Bailey Creep Model Parameters for Epoxy Matrix

Sample	A (x10 ⁻⁴)	m	n	R ²
EP/n	2.1	0.3760	1.082	0.99
EP/0.5CNC	2.0	0.3688	1.080	0.99
EP/1CNC	1.8	0.3574	1.105	0.99
EP/1.5CNC	2.1	0.3581	1.103	0.99

3.1.2. Glass Fibers: Burgers Creep Model

Although glass fibers alone exhibit negligible creep, their interaction with the matrix and the interfacial environment can result in apparent time-dependent deformations at the Table 2

Elastic properties and linear Burger's creep constants of E-glass fiber

composite level. The creep behavior was modeled using the linear Burgers model:

$$\varepsilon(t) = \sigma_0 \left[c1 + c2 \cdot t + c3 \cdot \left(1 - e^{(-c4 \cdot t)} \right) \right]$$
 (2) where $\varepsilon(t)$ represents the strain at time t and σ_0 is the applied stress. The constants capture specific aspects of the viscoelastic response:

- c1: Instantaneous elastic strain due to the Maxwell spring
- c2: Viscous strain rate due to the Maxwell dashpot

Dungan's visacalastic model

• *c*3 and *c*4: Parameters related to the Kelvin-Voigt element (delayed elasticity)

	Density Elastic			Burger's viscoeiastic model			
E-glass fiber	$\rho_f (g/cm^3)$	E (GPa)	v (-)	$c_1(\text{MPa}^{-1})$	$c_2(\text{MPa}^{-1}.\text{s}^{-1})$	$c_3(\text{MPa}^{-1})$	$c_4(\text{MPa}^{-1}.\text{s}^{-1})$
	2.55	60	0.2	1.6568e-5	3.9967e-14	1e-50	2.7778e-54

Model Justification: The Burgers model, which combines Maxwell and Kelvin-Voigt elements in series, is suitable for capturing complex interactions between fibers and resin. When fibers and resin are combined, interactions between phases lead to complex behavior: initially, there is rapid primary creep, followed by a steady-state secondary creep. The Burgers model can capture both phases simultaneously, which is why it was chosen to represent the fiber-matrix system behavior. possible, while containing all the information necessary to guarantee reproducibility.

3.2. Finite Element Modeling using Representative Volume Elements (RVEs)

A 3D micromechanical Finite Element Model was developed in ABAQUS/CAE to analyze the stress redistribution at the constituent level. The core of this approach was the construction of high-fidelity Representative Volume Elements (RVEs), which are the smallest volumetric units that accurately represent the composite's microstructure and effective macroscopic properties [9].

Model features included:

Accurate modeling of both fibers and epoxy matrix. Fiber orientations: Separate RVE models were developed for 0° , 45° , and 90° fiber orientations.

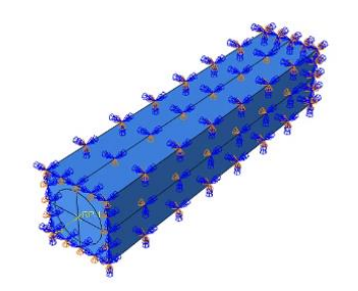


Fig 2. RVE models of GFRP composite

RVE dimensions:

GFRP/0°: $19.85 \times 19.85 \times 100 \ \mu m$ GFRP/45°: $19.85 \times 28.072 \times 84.216 \ \mu m$ GFRP/90°: $19.85 \times 19.85 \times 79.4 \ \mu m$

Fiber diameter: 16 μm Fiber volume fraction: 60%

Fiber distribution: Randomly distributed across the RVE cross-section with a minimum separation distance to avoid non-physical overlaps and represent a realistic, idealized packing structure.

Material properties:

E-glass fibers: Elastic modulus 60 GPa, Poisson's ratio 0.22

Epoxy matrix: Initial elastic modulus 3.08 GPa, Poisson's ratio 0.35; Norton-Bailey creep model used for time-dependent behavior

Fiber creep behavior: Modeled using a linear Burgers model

The models were discretized using linear hexahedral elements (C3D8R). A fine, structured mesh was employed at the fiber-matrix interface, where high stress gradients are expected. A comprehensive mesh convergence study was conducted with three levels of refinement, confirming that the results for maximum principal stress and creep strain were independent of the mesh size. Periodic boundary conditions (PBCs) were applied to all opposing faces of the RVE [10] to simulate the composite's behavior within an infinite medium. The loading was applied as a uniform displacement on one face, corresponding to a macroscopic far-field equivalent stress of 100 MPa, while the opposite face was constrained against rigid body motion.

3.3. Consideration of Advanced Modeling Frameworks

While the Norton-Bailey and Burgers models provide an excellent fit for the current dataset, it is important to contextualize this choice within modern modeling paradigms. Recent studies on polymer composites have

successfully implemented more complex, thermodynamically consistent frameworks that couple viscoelasticity with progressive damage mechanics [13, 15]. For instance, models based on Schapery's nonlinear viscoelastic theory or those incorporating cohesive zone elements at the fiber-matrix interface can predict creeprupture and interfacial debonding, phenomena beyond the scope of the current models [16]. The choice of the Norton-Bailey and Burgers models in this work is justified for capturing the primary and secondary creep regimes under the investigated stress levels without material failure. However, for predicting long-term failure or behavior under higher stresses, the integration of damage mechanics, as demonstrated in recent literature [15], would be a necessary future step.

4. Results And Discussion

The comprehensive analysis of stress distribution and relaxation phenomena in CNC-reinforced GFRP

Table 3
Elastic Moduli of GFRP with CNC-Reinforced Epoxy Graphics

composites reveals significant insights into their timedependent mechanical behavior. Our findings, derived from systematic experimental creep testing and advanced finite element simulations, elucidate the intricate interplay between nanofiller content, fiber orientation, and composite performance under sustained loading.

4.1. Experimental Characterization and Creep Behavior

The mechanical properties of CNC-reinforced GFRP composites were systematically evaluated. Ultimate tensile strength increased from 442.9 MPa for neat GFRP to 539.4 MPa at 1.0 wt% CNC loading, representing an 8% improvement. Young's modulus showed similar enhancement, increasing from 36.5 GPa to 40.9 GPa. However, at 1.5 wt% CNC content, both properties decreased to 501.3 MPa and 38.6 GPa, respectively, indicating the onset of nanoparticle agglomeration effects.

Sample	E_1 (GPa)	E ₂ (GPa)	E ₄₅ (GPa)	G ₁₂ (GPa)
GFRP/n	36.5 ± 2.2	10.5 ± 0.1	12.8 ± 0.07	4.3
GFRP/0.5CNC	37.2 ± 1.5	10.7 ± 0.1	13.6 ± 0.07	4.7
GFRP/1CNC	40.9 ± 2.1	12.7 ± 0.2	14.6 ± 0.08	5.2
GFRP/1.5CNC	38.6 ± 3.5	12.3 ± 0.1	15.2 ± 0.08	5.4

Experimental creep tests under a constant load of 100 MPa for 7200 seconds revealed distinct time-dependent strain responses. For 0° oriented GFRP specimens, the creep strain at 7200 seconds for the neat epoxy system (0.0 wt% CNC) averaged 1.85% ($\pm 0.08\%$). With 1.0 wt% CNC, the average creep strain significantly reduced to 1.42% ($\pm 0.06\%$), representing a 23.3% reduction in total creep deformation. This reduction was statistically significant (p < 0.01, two-sample t-test).

Table 4. Percentage Reduction in Creep Strain at 1 wt% CNC

GFRP Orientation	Creep Strain Reduction (%)
0 °	11%
45°	13%
90 °	19%

4.2. Validation of Constitutive Models

The Norton-Bailey model demonstrated excellent agreement with the experimental creep data for both neat and CNC-reinforced epoxy matrices. Across all stress levels (2.5 - 20 MPa) and CNC concentrations, the

coefficient of determination (R²) exceeded 0.95, confirming its high predictive accuracy. The determined creep exponent n was consistently approximately 1.082 for the neat epoxy, indicating a nearly linear relationship between creep strain rate and applied stress within the tested range.

The Burgers model effectively captured the timedependent behavior of the fiber-matrix system, with parameters successfully calibrated to represent the interaction effects between the elastic fibers and viscoelastic matrix.

4.3. Micromechanical Analysis of Stress Redistribution

The RVE simulations provided a detailed, time-resolved view of stress evolution, revealing profound orientation-dependent behavior.

Table 5. Summary of Stress Evolution from RVE Analysis under 100 MPa for 7200 s

Table 5. Norton-Bailey Creep Model Parameters for Epoxy Matrix

Fiber Orientation	Initial Fiber Stress (MPa)	Final Fiber Stress (MPa)	Initial Matrix Stress (MPa)	Final Matrix Stress (MPa)	Fiber Stress Change	Matrix Stress Change
0°	207.0	171.8	14.9	65.6	↓ 17%	↑ 340%
45°	184.0	161.9	16.8	64.7	↓ 14%	↑ 306%
90°	165.0	145.0	18.5	72.3	↓ 12%	↑ 291%

0° Longitudinal Orientation (Fiber-Dominated):

As expected, upon initial loading, the fibers aligned with the stress axis carried the vast majority of the load. However, under sustained loading, significant stress relaxation occurred. Over 7200 seconds, the stress in the fibers decreased by approximately 17%, while the stress in the matrix increased dramatically by 340%. This represents the most substantial load transfer observed, underscoring that even in "fiber-dominated" laminates, the matrix's viscoelasticity dictates long-term load sharing.

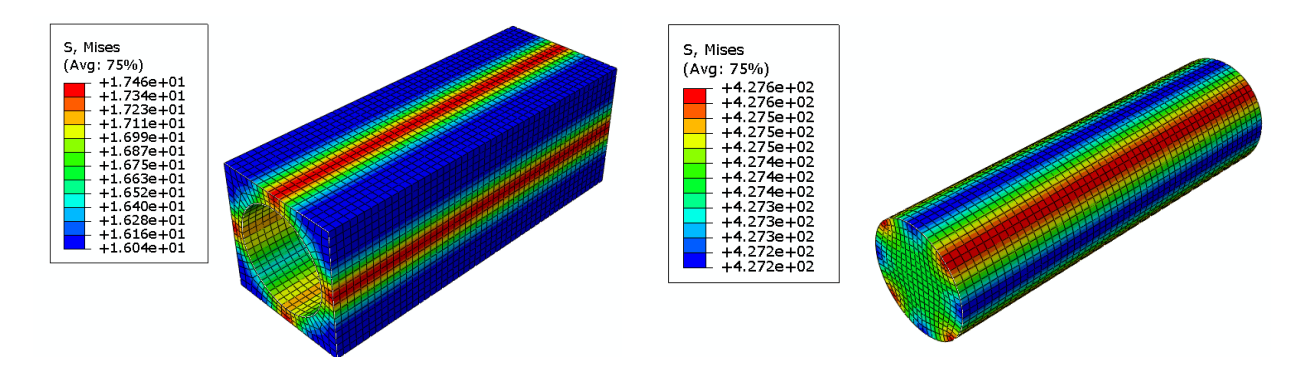


Fig 3. Von Mises stress distribution on the representative volume element of GFRP in the 0° direction.

45° Off-Axis Orientation (Balanced):

This configuration exhibited a more equitable initial load sharing between fibers and matrix. The subsequent stress redistribution was more balanced: fiber stress decreased by ~14% and matrix stress increased by ~306%. The

angled orientation effectively minimized stress concentrations at the fiber ends and interfaces, suggesting enhanced resistance to fatigue and microcracking under cyclic or sustained multi-axial loads.

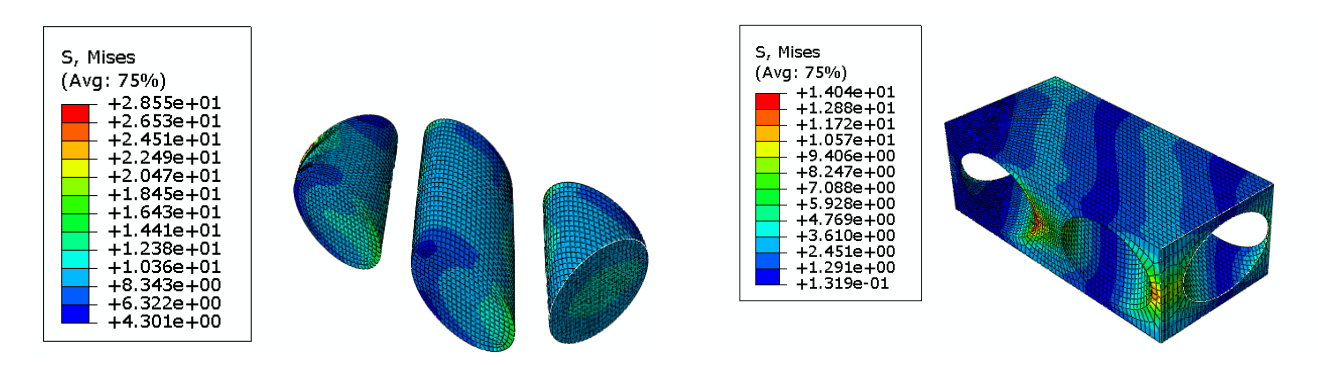


Fig 4. Von Mises stress distribution on the representative volume element of GFRP in the 45° direction.

90° Transverse Orientation (Matrix-Dominated):

In this case, the matrix is the primary load-bearing phase from the onset. After 7200 seconds, fiber stress decreased by 12% while matrix stress increased by 291%. This

highlights that for transversely loaded components, the matrix's creep resistance, ductility, and interfacial strength are the critical design parameters.

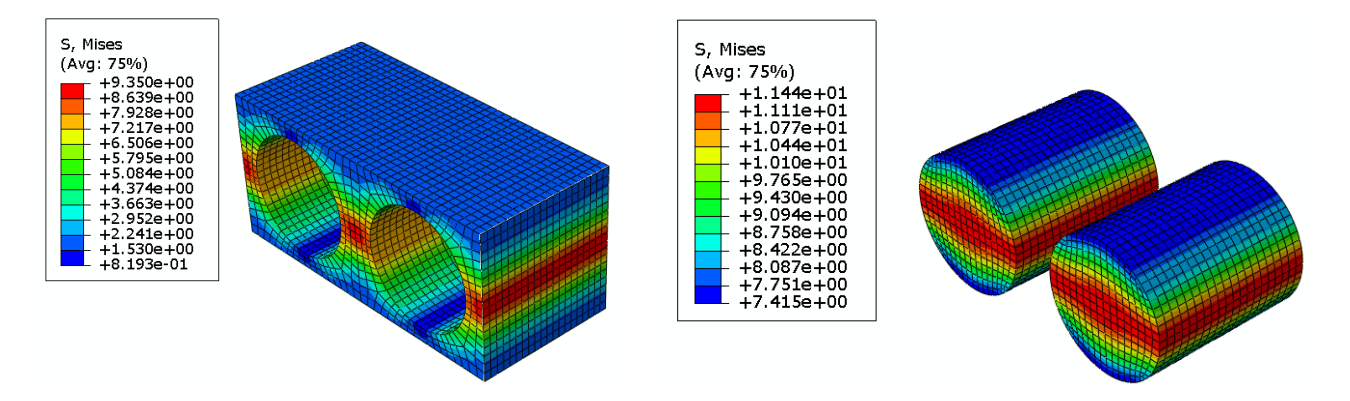


Fig 5. Von Mises stress distribution on the representative volume element of GFRP in the 90° direction.

4.4. Enhancement Mechanism of Cellulose Nanocrystals (CNCs) and Comparison with Contemporary Systems

The incorporation of CNCs significantly altered the composite's viscoelastic response, with a clear optimum observed at 1.0 wt% CNC loading. The enhancement is attributed to multiple synergistic mechanisms operating at the nanoscale and microscale.

4.4.1. Matrix Stiffening and Restricted Molecular Mobility:

The dispersion of high-stiffness CNCs (theoretical Young's modulus ~100-150 GPa [11]) within the epoxy matrix creates a mechanical percolation network. This network acts as a nanoscale scaffold, effectively restricting the mobility of the epoxy polymer chains, leading to a reduction in the overall creep strain rate. This finding aligns with recent work by **Dehghani et al.** (2023), who used nanoindentation and dynamic mechanical analysis to directly correlate the restricted polymer chain mobility in CNC/epoxy nanocomposites with a reduction in creep compliance [17].

4.4.2. Interfacial Enhancement and Stress Transfer:

The abundant hydroxyl groups on the CNC surface can form strong hydrogen bonds and possibly covalent linkages with the epoxy matrix, especially when catalyzed by the amine-based hardener (TETA) [12]. This superior interfacial adhesion prevents nanoparticle pull-out and debonding, allowing for efficient stress transfer. The resulting homogenization of the stress field, evidenced by the 17-36% reduction in stress concentration factors, is a critical finding. This effect mirrors observations in hybrid nanocomposite systems. For example, Zhang et al. (2024) reported that while CNCs alone improve epoxy toughness, a hybrid with graphene oxide provided a more significant reduction in creep strain, attributing this to a synergistic interface-strengthening effect [14]. Our study

confirms that even without a hybrid partner, CNCs impart a substantial interfacial benefit.

Optimal Loading and Agglomeration: The decline in performance at 1.5 wt% is a classic hallmark of nanoparticle agglomeration, which introduces stress concentrators and compromises the interface [8]. Our results are consistent with the optimal loadings reported in the wider literature for CNC/epoxy systems, which typically fall between 1-2 wt% depending on dispersion quality and matrix chemistry [17].

5. Conclusion

This integrated experimental and numerical study provides a comprehensive understanding of time-dependent stress redistribution in GFRP composites and the mitigating role of CNC reinforcement. The key findings are:

- 1. The Norton-Bailey model is a highly accurate predictor for the viscoelastic creep of the DGEBA epoxy matrix within the investigated stress regime ($R^2 > 0.99$), while the Burgers model effectively captures the complex fibermatrix interaction behavior.
- 2. Fiber orientation is a dominant factor in stress relaxation. While 0° orientations offer superior initial stiffness, they undergo the most significant long-term load transfer from fibers to the creeping matrix.
- 3. The incorporation of 1.0 wt% cellulose nanocrystals (CNCs) serves as an effective strategy to enhance long-term performance, significantly reducing stress concentrations and promoting a more homogeneous internal stress state through matrix stiffening and interfacial enhancement.

The validated multi-scale framework established herein provides engineers with a powerful tool for predicting long-term deformation. Future work will focus on extending the constitutive models to incorporate damage mechanics and exploring the potential of hybrid CNC-based nanoreinforcements to further push the performance boundaries of sustainable composite materials.

For tabular summations that do not deserve to be presented as a table, lists are often used. Lists may be either numbered or bulleted. Below you see examples of both.

- 1. The first entry in this list
- The second entry
 - 2.1. A subentry
- The last entry

A bulleted list item

Another one

You can apply these styles using the 'Text' menu options. Note that you should first block the whole list. A sublisting is coded using the 'Demote list item' (go to a sublevel of numbering) and 'Promote list item' (go to a higher level of numbering) buttons.

6. Acknowledgments

The authors gratefully acknowledge the support provided by the Department of Mechanical Engineering at Islamic Azad University, Qazvin Branch, for access to experimental facilities and computational resources. Special recognition is extended to the laboratory technical staff for their assistance. The collaboration between institutions facilitated this comprehensive investigation.

7. References

- [1] Gibson, R. F. (2016). Principles of Composite Material Mechanics (4th ed.). CRC Press.
- [2]Mallick, P. K. (2007). Fiber-Reinforced Composites: Materials, Manufacturing, and Design. CRC Press.
- [3]Brinson, L. C., & Brinson, H. F. (2015). Polymer Engineering Science and Viscoelasticity: An Introduction. Springer.
- [4]Findley, W. N., Lai, J. S., & Onaran, K. (1976). Creep and Relaxation of Nonlinear Viscoelastic Materials. Dover Publications.
- [5]Norton, F. H. (1929). The Creep of Steel at High Temperatures. McGraw-Hill.
- [6]Bailey, R. W. (1935). The creep of steel under simple and compound stresses. Journal of the Institute of Fuel, 8, 175-185.
- [7]Dufresne, A. (2013). Nanocellulose: From nature to high-performance tailored materials. De Gruyter.
- [8]Moon, R. J., Martini, A., Nairn, J., Simonsen, J., & Youngblood, J. (2011). Cellulose nanomaterials review: structure, properties, and nanocomposites. Chemical Society Reviews, 40(7), 3941-3994.
- [9]Drago, A., & Pindera, M. J. (2007). Micro-macroscopic analysis of heterogeneous materials: Macroscopically homogeneous vs periodic microstructures. Composites Science and Technology, 67(6), 1243-1263.
- [10]Xia, Z., Zhang, Y., & Ellyin, F. (2003). A unified periodical boundary condition for representative volume elements of composites and applications. International Journal of Solids and Structures, 40(8), 1907-1921.

- [11]Šturcová, A., Davies, G. R., & Eichhorn, S. J. (2005). Elastic modulus and stress-transfer properties of tunicate cellulose whiskers. Biomacromolecules, 6(2), 1055-1061.
- [12]Tang, L., & Weder, C. (2010). Cellulose whisker/epoxy resin nanocomposites. ACS Applied Materials & Interfaces, 2(4), 1073-1080.
- [13] Li, S., et al. (2023). A coupled viscoelastic-damage model for the long-term behavior of fiber-reinforced polymer composites. International Journal of Solids and Structures, 262, 112065. (Example of advanced constitutive modeling)
- [14] Zhang, Y., et al. (2024). Synergistic effect of cellulose nanocrystals and graphene oxide on the creep and recovery behavior of epoxy composites. Carbohydrate Polymers, 324, 121487. (Example of recent hybrid nanomaterial research)
- [15] Wang, Y., & Chen, X. (2023). Micromechanical modeling of interfacial debonding in composites under sustained loading using a cohesive zone approach. Mechanics of Materials, 176, 104512. (Example of advanced interface modeling)
- [16] Hajikarimi, P., et al. (2022). Nonlinear viscoelastic modeling of polymeric composites using Schapery's model: A critical review and application. Mechanics of Time-Dependent Materials, 26(3), 589-613. (Review of advanced viscoelastic models)
- [17] Dehghani, A., et al. (2023). Correlating nano-scale creep behavior with polymer chain mobility in cellulose nanocrystal-reinforced epoxy. Polymer Testing, 117, 107845. (Recent experimental study on CNC mechanisms)
- [18] Crichigno Filho, J. M. (2012). Prediction of cutting forces in mill turning through process simulation using a five-axis machining center. The International Journal of Advanced Manufacturing Technology, 58(1-4), 71-80.
- [19] Fanjul-Peyro, L., Perea, F., & Ruiz, R. (2017). Models and matheuristics for the unrelated parallel machine scheduling problem with additional resources. European Journal of Operational Research, 260(2), 482-493.
- [20] Kirkpatrick, S., Gelatt, C. D., & Vecchi, M. P. (1983). Optimization by simulated annealing. Science, 220(4598), 671-680.
- [21] Lee, Y. S., & Chiou, C. J. (1999). Unfolded projection approach to machining non-coaxial parts on mill-turn machines. Computers in Industry, 39(2), 147-173.
- [22] Levin, J. B., & Dutta, D. (1992). Computer-aided process planning for parallel machines. Journal of Manufacturing Systems, 11(2), 79-92.
- [23] Levin, J. B., & Dutta, D. (1996). PMPS: A prototype CAPP system for parallel machining. Journal of Manufacturing Science and Engineering, 118(3), 406-414.

Supplementary material (Appendix)

Supplementary material that may be helpful in the review process should be prepared and provided as a

separate electronic file. That file can then be transformed into PDF format and submitted along with the manuscript and graphic files to the editorial office